Improved S Transform Based Fault Detection Method in VSC Interfaced DC System

Dongyu Li, *Student Member, IEEE*, Abhisek Ukil, *Senior Member, IEEE*, Kuntal Satpathi, *Member, IEEE*, Yew Ming Yeap, *Member, IEEE*

***Abstract*—The short circuit fault in the VSC based dc power system typically generates rapidly rising transient current which may have serious repercussions on dc grid operation and health of the integrated power electronic devices. Thus, the dc grid requires a high speed and robust fault detection for reliable system operation. With this regard, this paper proposes a fault detection method based on the S transform (ST) with adaptive adjustment. This improved ST is based on frequency-domain and is able to detect the fault condition within 0.3 ms. It consists of high-frequency detection, which is responsible for fast response due to high time resolution, and low-frequency screening which is used to differentiate faults from other transient conditions. Introducing a correction factor into a Gaussian function when computing ST could extract the high-frequency spectrum, while the low frequency spectrum information is still retained. The proposed method is validated with the multiterminal dc system developed in the OPAL-RT based real-time simulator. Additionally, its performance is tested with the point-to-point experimental dc test bed. Comparative analysis with other popular frequency-domain fault detection methods, namely, wavelet transform and short-time Fourier transform substantiates the effectiveness of this method.**

***Index Terms*—DC grid, DC power system, Fault detection, Frequency spectrum, HVDC, S Transform, Time-frequency analysis.**

I. Introduction

With the development of IGBTs, voltage source converter (VSC) [1] based conversion systems have promoted the advancements of high-voltage dc (HVDC) based transmission networks [2]. Such VSC based conversion systems have inherent advantages of being able to integrate emerging power sources and asynchronous power networks, easier control thus enabling economic long-distance transmission networks [3].

One of the major drawbacks of the VSC based generation system is its vulnerability to dc faults. During the dc faults, the dc-link capacitor discharges rapidly making the VSC defenseless. It may cause more serious damage to the dc power system and network components. Thus, shorter detection time is required which should be in the range of 2 ms [4]. This is more stringent than the requirement in ac networks.

Apart from the detection time, another challenge is the ability to differentiate high-impedance faults from the system transients such as sudden load changes etc [5]. This is necessary to avoid spurious tripping operations of the protection devices [6].

D. Li is PhD student in the Dept. of ECSE, The University of Auckland, Auckland, 1010, New Zealand, (email: dli313@aucklanduni.ac.nz).

A. Ukil (corresponding author) is Associate Professor in the Dept. of ECSE, The University of Auckland, 3 Grafton Road, Auckland 1010, New Zealand, (email: a.ukil@auckland.ac.nz).

K. Satpathi is a Research Fellow at the Nanyang Technological University, Singapore, (email: ksatpathi@ieee.org).

Y. M. Yeap is a Scientist at the Institute for Infocomm Research (I2R), Singapore, (email: yeap_yew_ming@i2r.a-star.edu.sg).

A. Literature Review

Compared to the time domain analysis marked by its simple computation, the frequency-domain analysis could provide better accuracy to differentiate various types of transient. The popular frequency-domain based dc fault detection methods are wavelet transform (WT) and short-time Fourier transform (STFT). Although WT shows an improved performance compared to time-domain methods like rate of change of current (ROC) [7], [8], directly applying the wavelet coefficients for fault detection requires large memory space and calculation time. Apart from that, output of wavelet transform depends on the selection of the mother wavelet which is a difficult task [9]. STFT is affected by various factors including sampling frequency, selection of window functions, window width, number of fast Fourier transform (FFT) points and the ripple components of current signals [10], [11]. Its inherent limitation is apparent since its fixed window width limits the available time-frequency resolution.

B. Objective of the Study: S Transform based Algorithm

S Transform (ST) was proposed by R.G. Stockwell in 1996 where a variable window size determined by the frequency is defined [12]. The window size becomes wider in the low-frequency band and shortens during the high-frequency band. This resilience is a valuable improvement of STFT due to its effectiveness to improve the frequency resolution at low frequencies and time resolution at high frequencies. In addition, based on the close relation to STFT, ST could be computed by using relatively simple FFT and inverse fast Fourier transform (IFFT) algorithms which makes it better than WT, while the calculation of WT is relatively complex since its base function is the mother wavelet rather than the sine function. These properties of the ST make it suitable for nonlinear and non-stationary signal analysis [13], and particularly for the analysis of dc fault transients [14]–[16]. However, the existing research in the ST-based dc fault analysis is still relatively elementary without effective way to extract the required spectrum information [14]. Also, most of the works reported are validated using simulated signals only [15], [16].

Therefore, in this paper, a ST-based analysis with specific improvement for dc fault detection is proposed providing clearer detection and better application prospects. Its effectiveness is verified on a simulated multi-terminal dc (MTDC) system and an experimental point-to-point (P2P) dc system.

The remainder of this paper is organized as follows. Section II presents the principle and computation method of original ST analysis, and how to improve it by introducing a correction factor to make it suitable for dc fault detection.

Section III explains the typical characteristics of dc fault current. Section IV illustrates test systems including a MTDC simulation model in OPAL-RT and an experimental platform of P2P dc system. Section V presents simulation and experimental results in various aspects, including the detection time, the sensitivity analysis, performance in islanded dc power system, the effect of noise, filtering and lightning disturbance, and the comparison with WT and STFT. Then discussion is given in Section VI followed by conclusion in Section VII.

II. ST Based Fault Detection Method

A. ST Definition

The time-frequency resolution of ST relies on the variation of frequency [12]. It is directly related to STFT expressed as,

$$STFT(\tau, f) = \int_{-\infty}^{+\infty} h(t)g(t-\tau)e^{-i2\pi ft}dt, \quad (1)$$

where $h(t)$ is the original signal, $g(t)$ is the window function. Due to the weight effect of $g(t)$ towards $h(t)$ at $t = \tau$, the signal is reserved near τ and suppressed away from τ. Therefore, the frequency distribution of $h(t)$ can be expressed at $t = \tau$.

If the window function is chosen as Gaussian window, the corresponding STFT can be written as

$$STFT^*(\delta, \tau, f) = \int_{-\infty}^{+\infty} h(t)\frac{1}{\sqrt{2\pi}\delta}e^{-\frac{(\tau-t)^2}{2\delta^2}}e^{-i2\pi ft}dt. \quad (2)$$

From eq. (2), width of the Gaussian window is determined by δ. In order to realize adaptive adjustment of window width according to the frequency distribution of the signal, δ is defined as

$$\delta(f) = \frac{1}{|f|}. \quad (3)$$

Therefore, the expression of ST, whose window width varies inversely with the signal frequency in continuous domain, is obtained as

$$S(\tau, f) = \int_{-\infty}^{+\infty} h(t)\left[\frac{|f|}{\sqrt{2\pi}}e^{-\frac{f^2(\tau-t)^2}{2}}e^{-i2\pi ft}\right]dt. \quad (4)$$

B. Linear Property of ST

The linear property of ST makes it be able to reliably analyze the signal with additive noise as

$$S\{data\} = S\{signal\} + S\{noise\}, \quad (5)$$

where $data(t) = signal(t) + noise(t)$.

C. Calculation Method of ST

In [19], ST is also written as the operation on Fourier spectrum $H(f)$ of $h(t)$.

$$S(\tau, f) = \int_{-\infty}^{+\infty}\left[H(f+f_a)e^{-\frac{2\pi^2 f_a^2}{f^2}}\right]e^{i2\pi f_a\tau}df_a, f \neq 0. \quad (6)$$

If we put $\tau \to jT$, $f \to \frac{n}{NT}$, $f_a \to \frac{m}{NT}$, T being the sampling period, then the discrete ST is obtained as

$$S\left[jT, \frac{n}{NT}\right] = \frac{1}{N}\sum_{m=0}^{N-1} H\left[\frac{m+n}{NT}\right]e^{-\frac{2\pi^2 m^2}{n^2}}e^{\frac{i2\pi mj}{N}}, n \neq 0. \quad (7)$$

Thus, in this paper, ST is computed by the following steps.

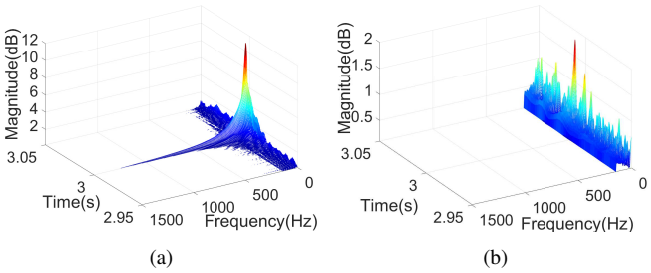

Figure 1. Time-frequency spectrum of original ST, (a) dc fault condition, (b) load change condition.

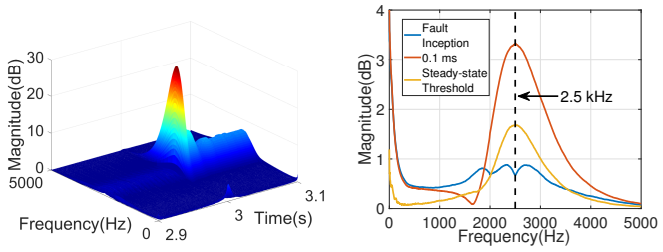

Figure 2. Time-frequency spectrum of improved ST, (a) three-dimensional graph, (b) two-dimensional graph.

1. Compute the FFT of h to get $H[\frac{m}{NT}]$, and $H[\frac{m+n}{NT}]$ by extension, where n is the number of frequency sampling points.
2. Compute the FFT of $g(t) = \frac{|f|}{\sqrt{2\pi}}e^{-\frac{t^2f^2}{2}}$ to get $G(m,n) = e^{-\frac{2\pi^2m^2}{n^2}}$.
3. Compute $H[\frac{m+n}{NT}]G(m,n)$ according to frequency sampling points.
4. Compute the IFFT of $H[\frac{m+n}{NT}]G(m,n)$ to get $S[jT, \frac{n}{NT}]$.

D. Fault Detection by ST

Due to its variable window width, ST is particularly useful for the dc fault detection since the spectrum information with high frequency resolution obtained in the low frequency band could distinguish the difference between various transients, while that with high time resolution in the high frequency band could detect the accurate moment when fault occurs.

As shown in Figure 1, the fault transient which occurs at 3.0 s could cause obvious spectral leakage in the low frequency band, while the spectrum of load change condition is relatively concentrated.

However, the poor time resolution in the low frequency band makes it hard to detect the accurate fault time from the original ST spectrum. In order to clearly observe the high frequency information with high time resolution, a correction factor ν is introduced into the Gaussian function in the Step-2 of ST calculation method mentioned previously. Its expression is modified as follow:

$$G(f_a, f) = e^{-\frac{2\pi^2(f_a-\nu)^2}{f^2}}. \quad (8)$$

Due to the weighting effect of Gaussian function, the spectrum information near ν is extracted. The value of ν should not be too low to obtain the required time resolution, and it should not be too high to suppress the spectrum information in the low frequency band. In this study, the sampling frequency is 10 kHz and ν is set as 2.5 kHz, the time-frequency spectrum of improved ST is shown in Figure 2.

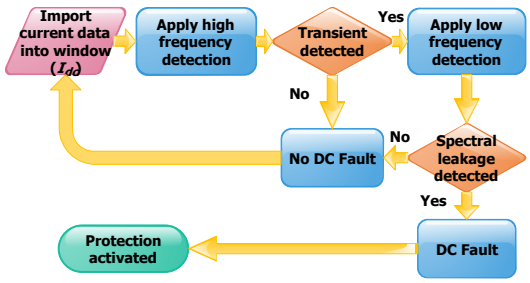

Figure 3. Flowchart of the proposed detection method.

As shown Figure 2(b), the high frequency information is extracted, while the low frequency information is still retained. The fault condition could be detected at 0.1 ms after the fault inception since both the magnitude near 2.5 kHz and that in the low frequency band exceed the steady-state threshold. Based on the improved ST analysis, the intact algorithm of proposed dc fault detection method should follow the flowchart in Figure 3.

III. Transients in DC Networks

A. DC Fault

Typical fault types vary in different dc grid systems. Pole-to-ground (PG) fault is most common in dc underground cable when its insulation is degraded and one conductor gets electrical contact with ground as shown in Figure 4(a) which illustrates a PG fault on the upper line and a resulting fault current loop involving the upper line, the upper dc capacitor and the neutral ground point. On the other hand, the dc overhead line is prone to occurrence of pole-to-pole (PP) fault due to direct exposure to air. This fault could result in most serious damage on the system due to complete discharge of dc-link capacitors and the extremely fast rising of fault current. As shown in Figure 4(b), PP fault would form a current loop involving the upper cable, the lower cable and the dc capacitor.

Due to the severity of PP fault, it is seen as the representative dc fault in this study. In the initial stage of PP fault, the dc-link capacitor discharging dominates the fault current, and the system characteristics could be regarded as the natural response of a RLC circuit. Under the condition $2R_{dc} + R_{f1} < 2\sqrt{2L_{dc}/C_{dc}}$, the capacitor discharging will cause an underdamped oscillation using the initial conditions $V_{dc}(t_0) = V_0$ and $I_{cap}(t_0) = 0$ as

$$I_{cap1}(t) = e^{-\delta t}(I_0 cos(\omega_1 t) + \frac{V_0/L - \delta I_0}{\omega_1} sin(\omega_1 t)), \quad (9)$$

where $\delta = \frac{2R_{dc}+R_f}{2(2L_{dc})}$, $\omega_0 = \sqrt{\frac{1}{2L_{dc}C_{dc}}}$ and $\omega_1 = \sqrt{\omega_0^2 - \delta^2}$. Under the condition $2R_{dc} + R_{f1} > 2\sqrt{2L_{dc}/C_{dc}}$, the discharging will cause an overdamped oscillation as

$$I_{cap2}(t) = Ae^{m_1 t} + Be^{m_2 t}, \quad (10)$$

where $m_{1,2} = -\delta \pm \sqrt{\delta^2 - \omega_0^2}$; $B = \frac{m_1 m_2}{m_1+m_2}(CV_0 - \frac{I_0}{m_1})$; $A = I_0 - B$. Then the fault current could be estimated by

$$I_{fault} = I_{dc} + I_{cap}. \quad (11)$$

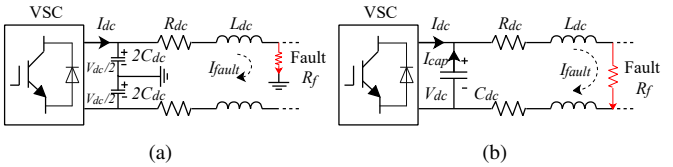

Figure 4. Equivalent fault current loop of (a) pole-to-ground fault and, (b) pole-to-pole fault.

TABLE I
Simulation Model Specification

System Parameter	Value
Number of terminals	7
DC capacitor	2350 μF
Steady state frequency	50 Hz
Sampling frequency	10 kHz
Cable length	$L_{12}, L_{13}, L_{23}, L_{24}, L_{34}$ $L_4, L_{45}, L_{46}, L_{47}$ = 50 km

TABLE II
Experiment Setup Parameters

Parameters	Values
Supply voltage	3ϕ, 85 V_{rms}, 50 Hz
3ϕ AC Protection Board	40 A, B Type, TP MCB with Shunt trip
3ϕ Variable Transformer	30 kVA, (0-415) V
Converters (VSC1, VSC2)	two-level 30 kVA, 400 V
DC Capacitor	C_{dc} = 2350 μF
DC Bus Voltage	V_{dc} = 120 V
DC Line Parameters	L_d = 1.5 mH, R_d = 0.03 Ω
DC MCB	C60H-DC, C 4 A
Interface Filter Parameters	R_f = 0.1 Ω, L_f = 10 mH
Linear Load	R_l = 20 Ω
Variable Power Resistor	5000 W, (1-16) Ω
DC Solid State Relay	D2D40, 200 V, 40 A

B. Other Transients

In HVDC systems, transients on a transmission line caused by the variation of grid load requirements or faults on other lines should not trigger the protection action on the monitored line. Therefore, it is necessary to differentiate these transients from fault transients.

IV. Test Systems For DC Fault Studies

A. Simulation Test System Description

The simulated MTDC system with hybrid topology is built in OPAL-RT as shown in Figure 5 [17], [18]. Its main system parameters are listed in Table I. Based on this model, PP dc faults on the dc line L_{12}, L_{13}, L_{23}, and PG dc faults on L_4, L_{45}, L_{47} are emulated with different fault resistances and distances from the terminal.

B. Experimental Test System Description

A P2P dc system is built as the hardware test setup in order to create load changing and dc fault transients. Its voltage level is scaled down for safety consideration. Figure 6 shows the schematic diagram of the experimental setup, and Table II lists parameters. This platform is supplied by 415 V, which is stepped down to 85 V (line-to-line rms) through a variable transformer (3-ϕ, 30 kVA, 0-415 V). VSC-1, which is used to rectify ac to dc, maintains the dc bus voltage at the level of 120 V. VSC-2 is assigned to control the ac voltage at the level of 50 V and supply power to 3-ϕ ac load. The voltage ($\pm$ 500 V to $\pm$ 15 V) and current ($\pm$ 10 A to $\pm$ 4 A) transducers based on Hall effect are applied to measure and convert the voltage and current values from power level to signal level. These signals are fed to the dSPACE 1103 controller to generate the

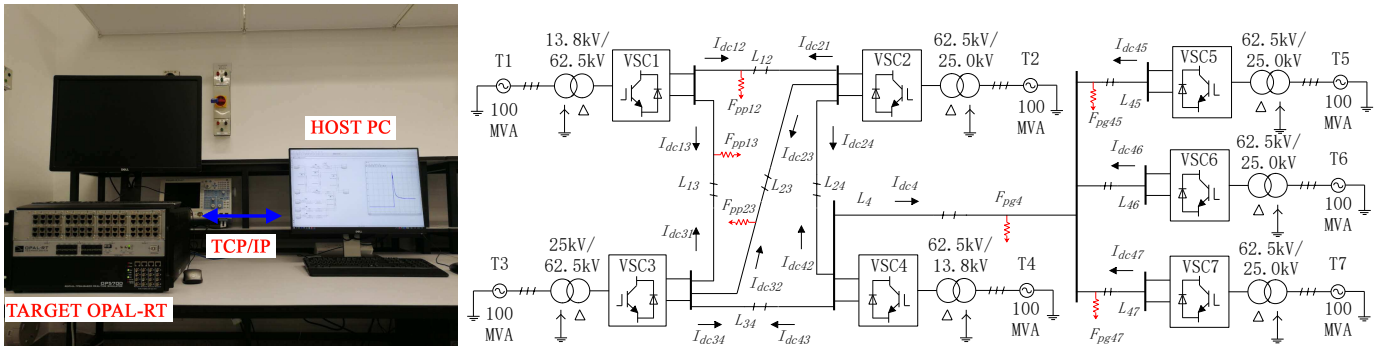

(a) (b)

Figure 5. Simulation test system (a) OPAL-RT setup and (b) schematic diagram of MTDC grid.

pulse-width modulation (PWM) control signals which are sent to drive circuits of VSC-1 and VSC-2.

The waveforms of PP dc fault and load changing in experiment are illustrated in Figure 7.

In order to prevent the short-circuit current from tripping the circuit breaker and causing the potential disturbance, PG faults and PP faults with low impedance is unfeasible to perform in this platform. Therefore, PP faults with relatively high impedance are studied in this paper and the fault resistance varies from 2 Ω to 14 Ω to produce different levels of dc fault currents. As for distance variation, different fault locations are simulated by changing the line inductance. Four emulated fault locations in the test are illustrated in Figure 8.

V. Simulation and Experimental Validation

The dc fault detection method consists of high-frequency detection providing fast identification speed, and low-frequency screening in case of the false positive caused by the sudden load change and the transient on fault-free lines.

A. Selection of Identification Frequency

In the high frequency detection, the closest point to ν, 2.485 kHz is chosen as the identification frequency and the steady-state threshold at this frequency point is set to 0.5004 dB in simulation, and 1.6725 dB in experiment by selecting the maximum value over a normal period.

As for the low frequency screening, the selection of identification frequency should consider the steady-state ripple which is different in simulation and experiment. Figure 9 shows the conventional ST spectrum of dc fault occurring at 3.0 s in the MTDC simulation system and the P2P experimental platform respectively. As can be seen, the frequency range of evident spectral leakage at the fault inception in simulation is different from that in experiment due to different frequency components contained in these two systems.

1) Simulation Test System: In the simulation test, the spectrum in the low-frequency band is relatively concentrated. The ripple frequency components in the dc prefault current signal are minimal and the frequency range of evident spectrum leakage for the fault-free line is limited to less than 50 Hz as shown in Figure 10(a). Therefore, the identification frequency should be greater than 50 Hz in simulation for low frequency screening algorithm in order to differentiate the fault-free line and the fault line.

2) Experimental Test System: As for experiment, the frequency distribution is more decentralized caused by complex frequency components. Among them, the most significant ripple is 150 Hz third harmonic component caused by other power electronics-based hardware testbed connected to the same 50 Hz ac supply. Therefore, the evident spectral leakage in the steady state mainly occurs within 150 Hz as shown in Figure 9(b) and Figure 10(b). The identification frequency in the experiment should be greater than 150 Hz.

In order to adopt unified identification frequency for the low frequency screening in both simulation and experiment, it should be chosen as a value greater than 150 Hz. A too large value is also unacceptable since the spectral leakage becomes less obvious in the high frequency band from the spectrum of original ST. In this paper, the identification frequency is 200 Hz and the steady-state threshold is set to 0.0937 dB and 0.0986 dB for simulation and experiment respectively.

B. Operation During Faults

When transients occur, the high frequency detection could provide fast response speed and the low frequency screening is responsible for differentiating whether the transient is normal or caused by a fault.

1) Simulation Spectrum Analysis: In the simulation, PP faults on L_{12}, L_{13}, L_{23} and PG faults on L_4, L_{45}, L_{47} with different fault resistances and locations are emulated. The frequency response of PP faults on L_{23} with low impedance (0.1 Ω) and high impedance (10 Ω) at 20 km from VSC2 is shown in Figures 11 and 12, and the transient on L_{12} caused by that fault with low impedance is analyzed in Figure 13.

From Figures 11 and 12, both the low impedance fault (LIF) and the high impedance fault (HIF) could be detected at 0.1 ms after the fault inception.

From Figure 13, although the transient current on L_{12} could make the high-frequency detection analysis result exceed the steady-state threshold, the low frequency screening algorithm could determine that the fault occurs beyond the line L_{12}.

2) Experimental Spectrum Analysis: In the experiment, analysis results of LIF (2 Ω), HIF (14 Ω) and load change are shown in Figures 14, 15, 16 respectively.

From Figures 14 and 15, both LIF and HIF could be detected at 0.1 ms after the fault inception.

As for the load change condition in Figure 16, the magnitude also exceeds the threshold at 5 ms after the switching action in the high-frequency band, but the magnitude obtained by using the low-frequency screening algorithm is only 0.0081 dB lower than the steady-state threshold 0.0986 dB. Therefore, load changing could be distinguished from fault transients.

C. Detection Time

With the variation of fault resistance and fault location, the amplitude and rising rate of fault current exhibit different

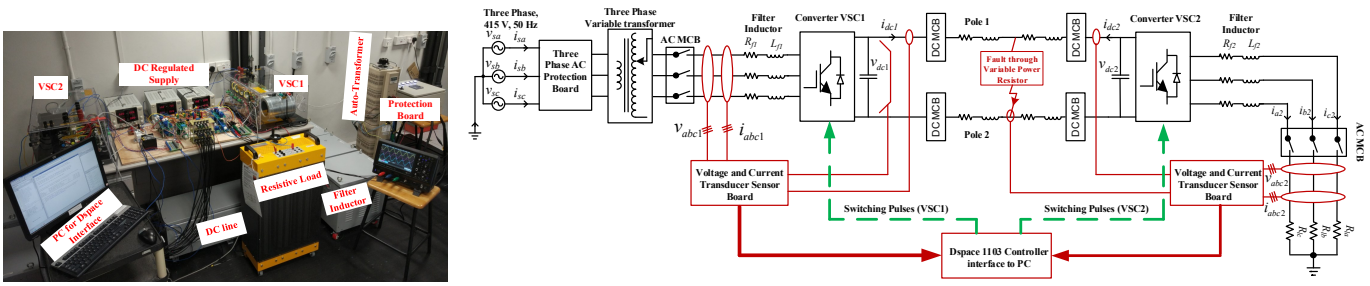

(a) (b)

Figure 6. Experimental test system (a) hardware setup and (b) schematic block diagram.

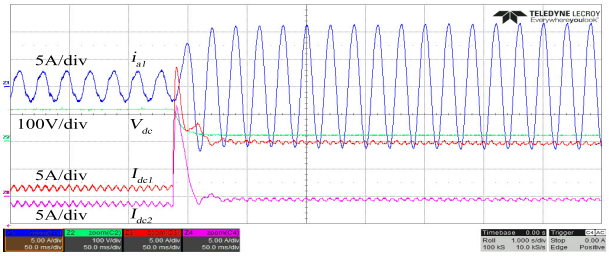

(a)

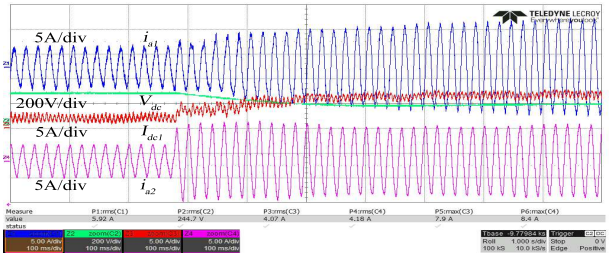

(b)

Figure 7. (a) Fault current waveform and (b) sudden load change in the experimental test system.

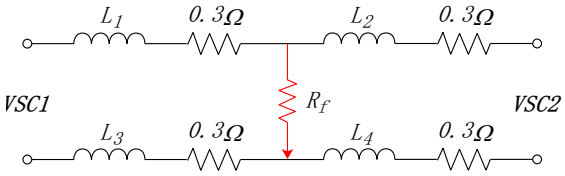

Location 1: L1, L2, L3, L4 = 2.8 mH.
Location 2: L1, L3 = 1.5 mH; L2, L4 = 2.8 mH.
Location 3: L1, L3 = 4 mH; L2, L4 = 1.5 mH.
Location 4: L1, L2, L3, L4 = 4 mH.

Figure 8. Fault locations and the corresponding line inductance.

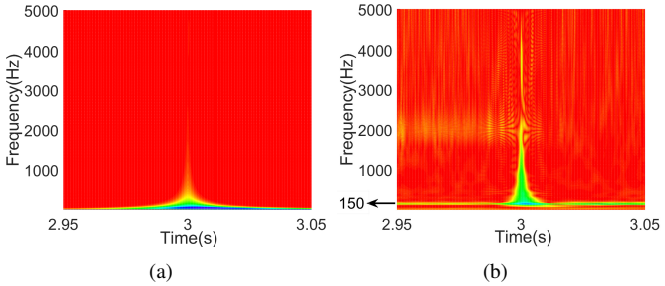

(a) (b)

Figure 9. Spectral leakage in the original ST spectrum of fault current in (a) MTDC simulation system, and (b) P2P experimental system.

features in both simulation model and experimental platform. Therefore, it is necessary to measure the effect of this change on the detection algorithm.

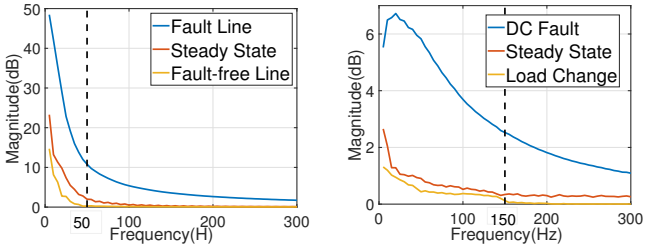

(a) (b)

Figure 10. Low frequency screening analysis results, (a) MTDC simulation system, and (b) P2P experimental system.

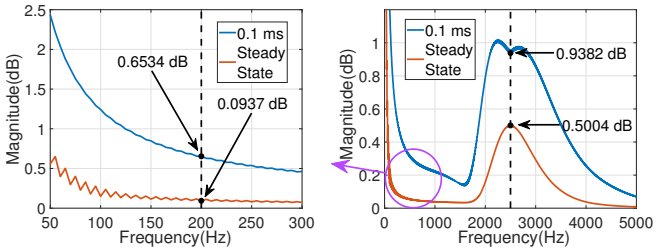

(a) (b)

Figure 11. Frequency response of simulated dc fault F_{pp23} with 0.1 Ω on L_{23}, (a) low frequency screening, (b) high frequency detection.

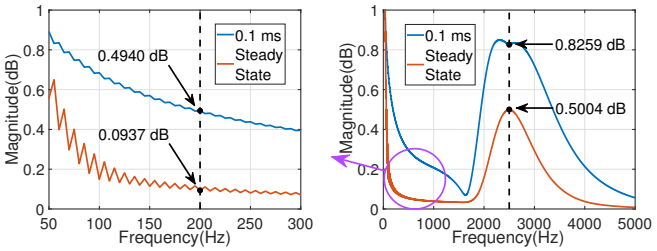

(a) (b)

Figure 12. Frequency response of simulated dc fault F_{pp23} with 10 Ω on L_{23}, (a) low frequency screening, (b) high frequency detection.

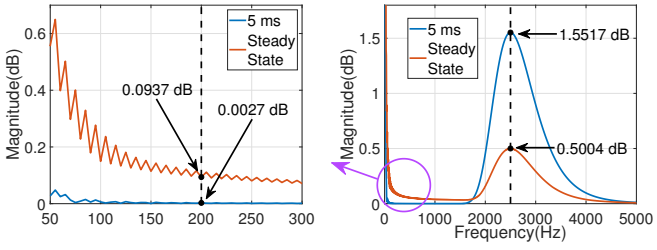

(a) (b)

Figure 13. Frequency response of simulated dc fault F_{pp23} with 0.1 Ω on L_{12}, (a) low frequency screening, (b) high frequency detection.

For the simulation test, the detection time for PP dc faults and PG dc faults with different fault resistances and distances from VSC1 on line L_{12} is summarized in Table III.

For the experimental test, the detection time with different

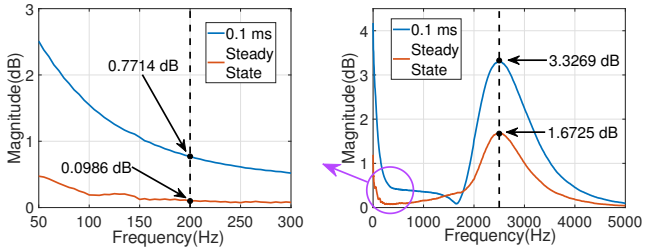

(a) (b)

Figure 14. Frequency response of experimental fault current with 2 Ω, (a) low frequency screening, (b) high frequency detection.

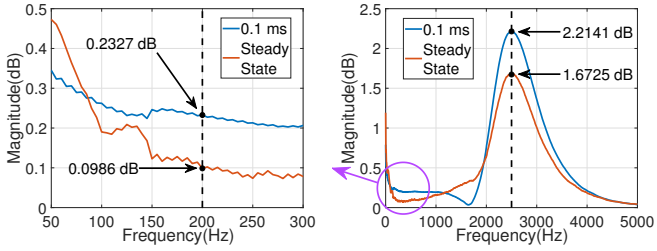

(a) (b)

Figure 15. Frequency response of experimental fault current with 14 Ω, (a) low frequency screening, (b) high frequency detection.

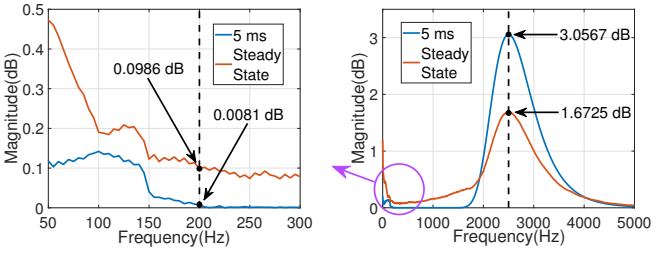

(a) (b)

Figure 16. Frequency response of experimental load change current, (a) low frequency screening, (b) high frequency detection.

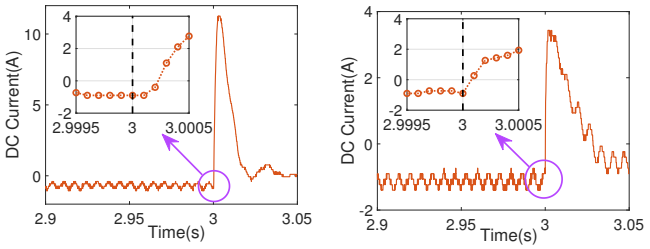

(a) (b)

Figure 17. The effect of ripple components on the detection time, (a) the fault occurs at the falling edge, (b) the fault occurs at the rising edge.

TABLE III
DETECTION TIME FOR SIMULATED DC FAULTS WITH VARYING FAULT LOCATIONS AND RESISTANCES

Fault Resistance	Fault Type	Fault Distance				
		10 km	*20 km*	*30 km*	*40 km*	*50 km*
0.1 Ω	PP	0.1 ms	0.1 ms	0.2 ms	0.2 ms	0.2 ms
	PG	0.1 ms	0.1 ms	0.2 ms	0.2 ms	0.2 ms
0.5 Ω	PP	0.1 ms	0.1 ms	0.2 ms	0.2 ms	0.2 ms
	PG	0.1 ms	0.1 ms	0.2 ms	0.2 ms	0.2 ms
1 Ω	PP	0.1 ms	0.1 ms	0.2 ms	0.2 ms	0.2 ms
	PG	0.1 ms	0.1 ms	0.2 ms	0.2 ms	0.2 ms
2 Ω	PP	0.1 ms	0.1 ms	0.2 ms	0.2 ms	0.2 ms
	PG	0.1 ms	0.1 ms	0.2 ms	0.2 ms	0.2 ms
5 Ω	PP	0.1 ms	0.1 ms	0.2 ms	0.2 ms	0.2 ms
	PG	0.1 ms	0.1 ms	0.2 ms	0.2 ms	0.2 ms
10 Ω	PP	0.1 ms	0.1 ms	0.2 ms	0.2 ms	0.2 ms
	PG	0.1 ms	0.1 ms	0.2 ms	0.2 ms	0.2 ms

fault resistances and locations is listed in Table IV. The performance by monitoring the negative pole is shown in Table V.

TABLE IV
ANALYSIS RESULTS FOR EXPERIMENTAL DC FAULTS WITH VARYING FAULT RESISTANCES AND LOCATIONS

Fault Resistance	Location 1		Location 2		Location 3		Location 4	
	Time	*Sensitivity*	*Time*	*Sensitivity*	*Time*	*Sensitivity*	*Time*	*Sensitivity*
2 Ω	0.1 ms	7.8225	0.1 ms	8.1773	0.2 ms	3.3118	0.1 ms	3.4562
4 Ω	0.1 ms	6.5992	0.1 ms	7.1522	0.1 ms	2.5307	0.1 ms	2.6606
6 Ω	0.1 ms	5.9790	0.1 ms	6.5317	0.1 ms	2.6881	0.1 ms	2.8898
8 Ω	0.1 ms	6.2357	0.1 ms	6.0916	0.1 ms	2.5272	0.1 ms	2.7935
10 Ω	0.1 ms	4.6470	0.1 ms	6.3580	0.1 ms	2.6338	0.1 ms	2.8909

TABLE V
ANALYSIS RESULTS BY MONITORING BOTH POSITIVE POLE AND NEGATIVE POLE IN EXPERIMENT AND SIMULATION

Fault Resistance	Monitored Pole	Experimental PP fault		Simulated PG fault	
		Time	*Sensitivity*	*Time*	*Sensitivity*
2 Ω	Positive	0.2 ms	5.9482	0.1 ms	5.4777
	Negative	0.3 ms	6.8611	–	**0.7864**
4 Ω	Positive	0.1 ms	4.6952	0.1 ms	5.3689
	Negative	0.1 ms	5.3667	–	**0.7877**
6 Ω	Positive	0.1 ms	4.0885	0.1 ms	5.2277
	Negative	0.1 ms	4.8175	–	**0.7894**
8 Ω	Positive	0.1 ms	3.9517	0.1 ms	5.0628
	Negative	0.1 ms	4.5712	–	**0.7909**
10 Ω	Positive	0.1 ms	3.5184	0.1 ms	4.8821
	Negative	0.1 ms	4.2811	–	**0.7917**
12 Ω	Positive	0.1 ms	3.2858	0.1 ms	4.6918
	Negative	0.1 ms	3.8683	–	**0.7937**
14 Ω	Positive	0.1 ms	2.3596	0.1 ms	4.5000
	Negative	0.1 ms	2.9918	–	**0.7940**

TABLE VI
SENSITIVITY FOR SIMULATED PP AND PG DC FAULTS WITH VARYING FAULT LOCATIONS AND RESISTANCES

Fault	Loc (km)	Res (Ω)	Sensitivity						Reliable (?)
			I_{dc12}	I_{dc13}	I_{dc23}	I_{dc4}	I_{dc45}	I_{dc47}	
F_{pp12}	10	0.1	**17.0805**	0.2425	0.0631	0.4839	0.5370	0.2566	Yes
	10	1	**16.7327**	0.2285	0.0245	0.4264	0.0539	0.0609	Yes
	10	10	**10.3837**	0.0511	0.0142	0.0997	0.0068	0.0631	Yes
F_{pp13}	20	0.1	0.1785	**5.0768**	0.1305	0.5221	0.5110	0.2417	Yes
	20	1	0.1821	**5.0604**	0.0450	0.4297	0.0630	0.0610	Yes
	20	10	0.0398	**3.8246**	0.0117	0.1002	0.0071	0.0633	Yes
F_{pp23}	30	0.1	0.1542	0.0327	**2.8459**	0.7595	0.4292	0.4219	Yes
	30	1	0.0975	0.1324	**2.8811**	0.5414	0.1187	0.1285	Yes
	30	10	0.0173	0.0160	**2.6778**	0.1280	0.0400	0.0379	Yes
F_{pg4}	10	0.1	0.0514	0.0547	0.0036	**5.2066**	0.3938	0.3578	Yes
	20	0.1	0.1041	0.0983	0.0068	**2.1905**	0.3914	0.3577	Yes
	30	0.1	0.1066	0.1000	0.0075	**1.0671**	0.3813	0.3500	Yes
F_{pg45}	10	1	0.0205	0.0139	0.0098	0.2925	**5.3478**	0.3730	Yes
	20	1	0.0477	0.0399	0.0107	0.3050	**2.2067**	0.3734	Yes
	30	1	0.0650	0.0624	0.0073	0.3230	**1.0305**	0.3638	Yes
F_{pg47}	10	10	0.0198	0.0206	0.0014	0.3911	0.3858	**5.1379**	Yes
	20	10	0.0185	0.0220	0.0032	0.3926	0.3912	**2.1600**	Yes
	30	10	0.0190	0.0215	0.0026	0.3852	0.3821	**1.0510**	Yes

It can be concluded the typical detection time of this ST based algorithm is within 0.2 ms in both simulation and experiment. However, the ripple component in the hardware testbed may cause a delay in the detection time. As shown in Figure 17(a), if the fault occurs at the falling edge of the ripple component, the current does not distort until 0.3 ms after the fault inception. In comparison, the dc line current starts to distort from the very beginning at 0.1 ms after the fault inception if the fault occurs at the rising edge of the ripple component, as shown in Figure 17(b). Therefore, each test may produce different detection time from that obtained under the same experimental conditions. However, even with this delay, this novel method could detect LIFs and HIFs within 0.3 ms.

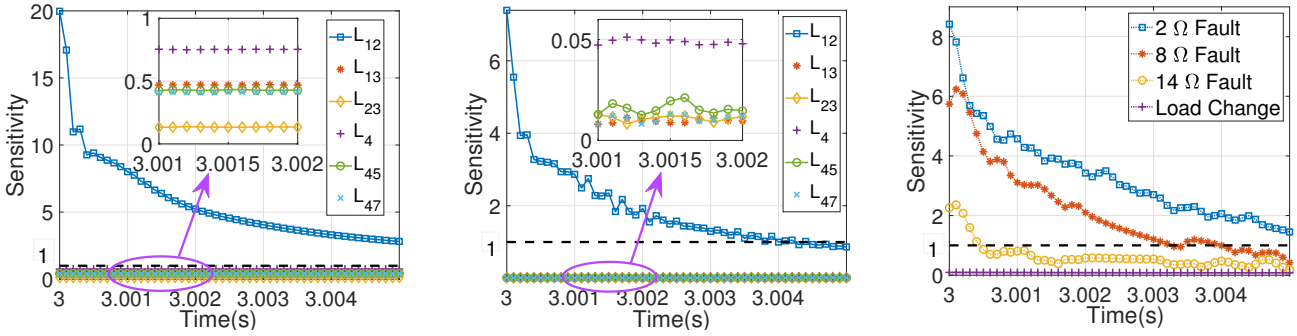

(a) (b) (c)

Figure 18. Time-variation sensitivity of, (a) PP faults in MTDC simulation system, (b) PG faults in MTDC simulation system, and (c) P2P experimental system.

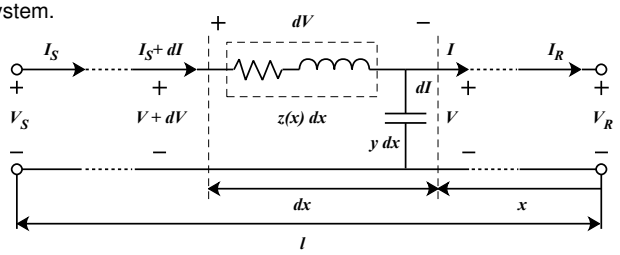

Figure 19. Transmission line model with distributed parameters.

TABLE VII
SENSITIVITY PERFORMANCE ON DISTRIBUTED LINE AND SERIES RL LINE IN OPAL-RT

	Distributed Line			Series RL Line		
	0.1 Ω	*1 Ω*	*10 Ω*	*0.1 Ω*	*1 Ω*	*10 Ω*
I_{dc12}	**2.7874**	**2.6854**	**1.6515**	**2.3846**	**2.2803**	**1.4484**
I_{dc13}	0.3181	0.0237	0.0020	0.3454	0.0256	0.0019
I_{dc23}	0.2053	0.0212	0.0022	0.2216	0.0228	0.0023
I_{dc4}	0.0563	0.0020	0.0003	0.0686	0.0040	0.0008
I_{dc45}	0.0188	0.0007	0.0001	0.0229	0.0013	0.0003
I_{dc47}	0.0188	0.0007	0.0001	0.0229	0.0013	0.0003

D. Sensitivity Analysis

The sensitivity of a specific fault detection method is defined as follow [7]:

$$Sensitivity = \frac{\omega_t}{\omega_{ss}}, \tag{12}$$

where ω is the value of identification parameter, and the subscripts t and ss indicate the transient condition and the steady-state respectively. A small value of ω_t, which means $sensitivity < 1$, represents the invalidation of a fault detection method.

The sensitivity of this proposed method in this paper is calculated based on the low-frequency screening algorithm. In the MTDC simulation test system, the sensitivity of PP faults and PG faults on different lines with the variation of fault resistance and fault location is shown in Table VI. Although the sensitivity is impaired by the increase of fault resistance and distance from the monitoring terminal, the fault line still could be detected correctly in all cases.

In the P2P experimental test system, the sensitivity of faults with different fault resistances and different locations is illustrated in Table IV, and the sensitivity of faults with different fault resistances by monitoring different poles is illustrated in Table V. Although an overall downward trend could be noticed with the increase of fault resistance and distance, the sensitivity remains above 1 which is high enough for correct fault detection.

In addition, the proposed method is able to correctly identify the faulted pole when PG faults occur. The analysis results of simulated PG faults on the positive pole are shown in Table V. From the table, experimental PP faults could be identified if both the positive pole and the negative pole detect the fault transient, while the simulated PG faults cause that the fault transient only be detected in the positive pole.

Moreover, the time-variation sensitivity of PP fault on line L_{12} in the MTDC simulation test system with 0.1 Ω at 10 km from VSC1 is shown in Figure 18(a), and that of PG fault is shown in Figure 18(b). The sensitivity of transients on line L_{12} maintains at the high level greater than 1 after the fault occurs at 3.0 s, while the sensitivity analysis results of other lines are lower than 1 over the entire period.

The time-variation sensitivities of PP faults in the P2P experimental test system with different fault resistances and the load change condition are shown in Figure 18(c). The sensitivity of HIF could maintain above 1 until 0.4 ms after the fault occurrence, which is enough for the accurate detection. However, the load change condition would not be identified as the fault transient since the sensitivity analysis results of load change are lower than 1 over the entire period.

E. Application in Islanded DC Power System

In the islanded dc power system like dc microgrids, shipboard/aircraft power networks etc, fault detection becomes challenging using traditional approaches. In the islanded microgrid, the fault current level is considerably smaller as compared to the grid-connected mode [19]. In the dc shipboard power system, due to its smaller scale and more complex multi-terminal distribution network, it is difficult to detect the fault location accurately [20].

The synchronous generators of simulated MTDC system in OPAL-RT are replaced by distributed generators with 380 V, 50 kW [21] to emulate the islanded dc grid. The transmission lines respectively adopt the distributed parameters lines illustrated in Figure 19 to simulate the general dc grid, or series R-L circuits whose configuration is similar to that in Figure 8 to emulate the small scale power system in the dc shipboard. The electrical parameters of the distributed transmission line are chosen as 0.01273 Ω/km, 0.9337×10^{-3} H/km and 12.74×10^{-9} F/km. The resistance and inductance of the series R-L circuit are selected as 0.1 Ω and 0.01 H.

PP faults with different fault resistances are set on the line L_{dc12} at 10 km from VSC1 in the dc system with distributed transmission line, or the midpoint in the system with series R-L circuits. Faults on both line models could be detected at 0.1 ms after the fault inception. In addition, Table VII shows

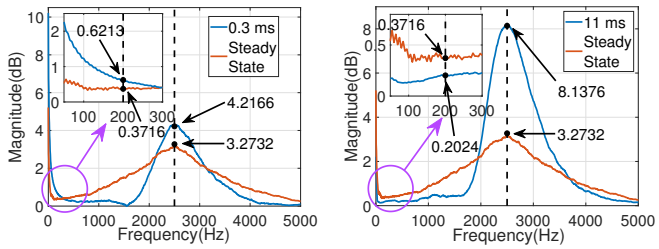

(a) (b)

Figure 20. Frequency response of simulated dc fault F_{pp23} with 1 Ω (signal-plus-Gaussian-white-noise) on (a) I_{23}, and (b) I_{12}.

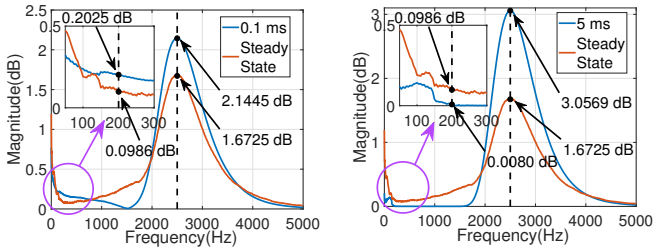

(a) (b)

Figure 21. Frequency response of experimental current signals after filtering, (a) 14 Ω fault, (b) load change.

that there is no significant distinction between the sensitivity analysis results of both models. Moreover, the fault line with various fault resistance could always be identified from fault-free lines. Therefore, the performance of this detection method is least affected by the existence of distributed capacitance, and the measure of using series R-L elements to simulate different fault locations in the P2P dc system is effective.

F. Effect of Noise and Filtering

Since the background noise and the filtering operation could influence the frequency spectrum distribution, some frequency-domain based fault detection methods are vulnerable to the noise effect such as STFT [8]. For an effective method, it should maintain its robustness against the noise and filtering. These effects on ST are evaluated in this subsection.

1) Noise Effect in Simulation: In the simulation test system, white Gaussian noise is added into the original signal of I_{12}, I_{23} when the PP fault occurs on L_{23} with 1 Ω fault resistance.

From Figure 20(a), the dc fault condition can still be detected at 0.3 ms after the fault inception although the noise causes a certain degree of spectrum distortion.

Figure 20(b) shows the ST analysis result on I_{12}. Although the analysis result exceeds the steady-state threshold at 11 ms after the fault inception in the high frequency band, the low frequency analysis result could always guarantee that L_{12} would not be detected as the fault line.

As shown, the noise slows the detection speed and reduces the sensitivity. However, a suitable adjustment of steady-state threshold could still guarantee the correctness of this detection method.

2) Filtering Effect in Experiment: As the aforesaid discussion, the noise condition could cause detection delay and sensitivity decline due to the dominant ripple frequency in steady state. Therefore, it may be needed to filter the original signal to get a better detection performance in the practical application.

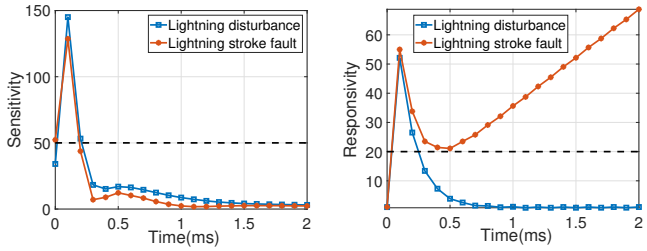

(a) (b)

Figure 22. Analysis results on the lightning surge of 0.25/100 μs, (a) Time-variation sensitivity, (b) Time-variation responsivity.

TABLE VIII
ANALYSIS RESULTS ON FOUR LIGHTNING SURGES

Lightning Surges	Lightning Disturbance		Lightning Stroke Fault		Reliable (?)
	Sensitivity	*Responsivity*	*Sensitivity*	*Responsivity*	
0.25/100 μs	145.0569	**1.1085**	128.6646	35.6433	Yes
1.2/50 μs	72.5886	**0.0803**	57.2792	35.4960	Yes
2.6/50 μs	71.9431	**0.0799**	56.6310	35.4957	Yes
10/350 μs	206.7144	**13.8095**	192.4642	49.2290	Yes

In this paper, the wavelet denoising method is used to filter the current signal under the 14 Ω fault condition and the load change condition in the P2P experimental setup. The wavelet basis function is selected as db3. The analysis results on the PP dc fault and the load change are shown in Figure 21.

In Figure 21(a), the dc fault condition could be detected at 0.1 ms after the fault inception with the sensitivity of 2.0538, while the normal sensitivity is 2.3596 without filtering. Therefore, the filtering operation almost does not change the performance of proposed method.

Moreover, Figure 21(b) shows that the load changing would not be identified as the fault transient regardless of filtering.

Therefore, the proposed method is less affected by the noise and filtering. This is because ST is a linear time-frequency analysis method without the interference of cross terms shown in eq. (5), and ST spectrum could preserve its high quality after adding noise or filtering. The negative effect of noise could be eliminated by adjusting the steady-state threshold, while the detection effect of proposed method basically remains unchanged after filtering.

G. Effect of Lightning Disturbance

Based on the international standard IEC 62305-1:2006, four lightning surges, including 0.25/100 μs, 1.2/50 μs, 2.6/50 μs and 10/350 μs [22] are injected into the simulated system. As shown in Figure 22(a), the lightning surge could be distinguished from the fault transient based on its extremely high sensitivity. In order to differentiate the lightning stroke fault from the lightning disturbance, responsivity is introduced whose definition formula is similar to that of sensitivity as follow:

$$Responsivity = \frac{m_t}{m_{ss}}, \tag{13}$$

where m is the magnitude of improved ST spectrum at ν, and the subscripts t and ss indicate the transient condition and the steady-state respectively.

Compared with the sensitivity, the responsivity could accurately reflect the charactersitics change of signal in time domain. This is the main difference between the lightning

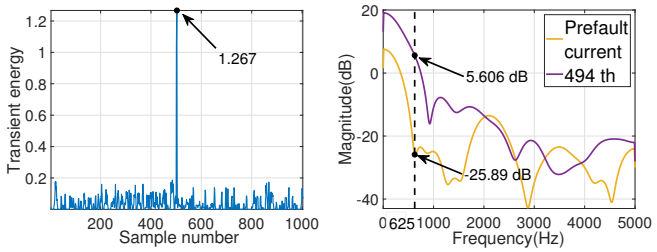

(a) (b)

Figure 23. Frequency response of experimental dc fault with 2 Ω at Location 2, (a) WT, (b) STFT.

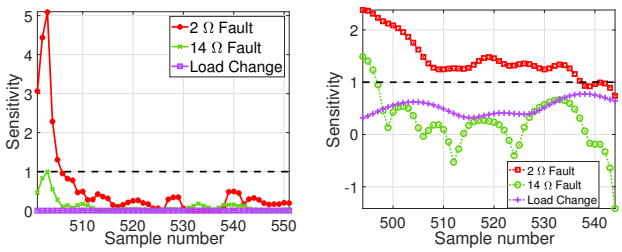

(a) (b)

Figure 24. Time-variation sensitivity after fault inception by using (a) WT or (b) STFT.

disturbance and the lightning stroke fault as shown in Figure 22(b) since the lightning stroke could cause the short-circuit fault subsequently.

In this paper, the sensitivity threshold at 0.1 ms after the fault inception is set as 50 and the responsivity threshold at 1 ms after the fault inception is set as 20. The analysis results of proposed method on four lightning surges are shown in Table VIII. It is evident that the lightning disturbance or the lightning stroke fault could always be differentiated from each other and the general fault transient.

H. Comparison with WT and STFT

In order to illustrate the effectiveness of this ST based fault detection method, its performance is compared with other frequency-domain fault detection methods, namely, WT and STFT. This comparison is based on the dc fault current produced on the experimental test system.

WT analysis is performed by using db3 as mother wavelet, since it provides the best match for the given fault pattern [8]. As for the decomposition process, scale-1 is selected since this level contains the highest frequency components [23], [24]. The criterion to identify the dc faults is the transient energy defined as follow [23]:

$$E_h = \int_0^{T_\omega} d_j[n]^2 dt > E_{set}, \tag{14}$$

where $d_j[n]$ represents the detailed coefficients of current signal at j–level, T_ω is the time window and E_{set} is setting threshold value. In this paper, T_ω is set as 0.3 ms and E_{set} is set as 0.25.

For STFT analysis, Hanning window with 32 samples window length is selected, since that is minimally affected by noise according to [8].

With regard to dc fault detection, WT is based on the high value of transient energy which is caused by high frequency components in the transient signal, whereas STFT is based on the increased magnitude at the update-frequency as shown in Figure 23.

1) Recognition Speed: In most cases, WT using scale-1 decomposition could detect the fault at 503th sample with detection time of 0.1996 ms. For STFT, the identification frequency is chosen as 625 Hz and the threshold magnitude is set as -10 dB. By applying STFT method, dc faults normally could be detected at 494th sample with detection time of 0.2033 ms. Therefore, this ST method consumes the least detection time as its typical detection time of ST method is 0.1 ms as shown in Table IV and Table V.

2) Discrimination Between Fault Transients and Normal Transients: Figure 18 and Figure 24 compare the sensitivity performance of these three detection methods on LIF, HIF and load changing.

As shown, HIF would make WT lose its effectiveness since its sensitivity is less than 1 in that situation. STFT could keep its validity to differentiate both LIF and HIF from the load change condition. However, the STFT sensitivity of load change fluctuates and that result is close to 1 which reduces the discrimination between normal transients and fault conditions. This characteristic indicates that the detection performance of STFT is vulnerable to the noise interference.

In contrast, ST method could always be effective in case of LIF or HIF, and the discrimination between load change and fault conditions is distinctive in Figure 18.

3) Robustness Against Change of Fault Conditions: Table IX shows the sensitivity of different fault resistances and locations by using WT or STFT. The sensitivity of WT is greatly influenced by fault conditions, and even in some cases, it will lose its effect. This is caused by the decline of instantaneous frequency of fault current with the increase of fault resistance and distance from the terminal. However, STFT performs the greatest robustness as its sensitivity is almost unchanged with the variation of fault resistance and location.

From Table IV, although the sensitivity of ST varies with fault conditions, this novel method could maintain its validity in all the experimental test. In this respect, the highest rank is STFT followed by ST and WT.

4) Failure Rate: As aforesaid discussion, WT may fail in case of HIF. Detailed performance of these three methods is shown in Table IV and Table IX. As shown, in all 20 cases, WT loses its validity in 9 cases as the sensitivity is less than 1. Although increasing the decomposition iterations to obtain the information at the lower frequency level could solve this problem in these cases, the recognition speed would be greatly dragged down. For instance, the typical detection time of scale-3 WT is 0.7905 ms in the hardware test.

In contrast, both STFT and ST could take effect in all cases. Therefore, the failure rate of WT, STFT and ST could be estimated to be 45%, 0 and 0 respectively.

5) Calculation Burden: The calculation burden of these three methods is evaluated on a 32-bit DSP TMDSC-NCD28335 with 150 MHz clock which equates to 6.67 ns per instruction. The time series signal with 64 points is input into the algorithms. The core functions of WT, STFT and ST cost 159370, 76891, and 138947 clock cycles in instruction

TABLE IX
SENSITIVITY FOR EXPERIMENTAL PP FAULTS BY USING WT OR STFT

Fault Resistance	Location 1		Location 2		Location 3		Location 4	
	WT	*STFT*	*WT*	*STFT*	*WT*	*STFT*	*WT*	*STFT*
2 Ω	5.0880	2.3807	5.0680	2.3896	**0.4968**	1.8961	1.0788	1.9821
4 Ω	3.2092	2.2530	1.9588	2.2832	**0.6952**	1.7433	**0.3865**	1.8410
6 Ω	3.5968	2.1502	3.8132	2.2229	**0.5040**	1.7551	**0.7668**	1.8050
8 Ω	1.1096	2.1608	1.5924	2.1628	**0.7704**	1.7078	**0.8340**	1.8223
10 Ω	**0.5772**	2.0191	3.2540	2.1762	2.6448	1.6721	**0.4912**	1.7926

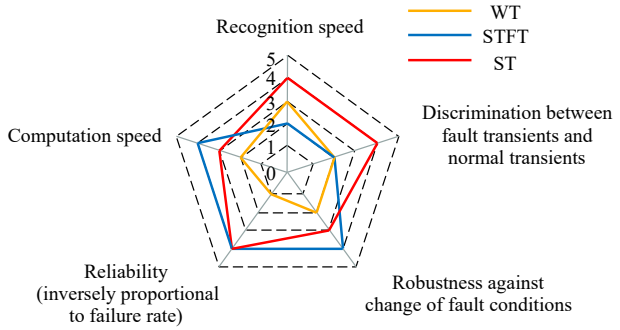

Figure 25. Performance comparison between WT, STFT and ST (rank 5 is most desirable and rank 0 is least desirable).

operations, which are the equivalent of 1.0625 ms, 0.5126 ms, and 0.9263 ms respectively. As shown, STFT is the fastest method followed by ST and WT. Although the necessity of executing both FFT and IFFT puts a drag on calculation speed of ST, the sum of its detection time and calculation time is always within 1.3 ms (< 2 ms) under different fault conditions. Therefore, the proposed method is suited for dc fault detection.

VI. DISCUSSION

It has been demonstrated that the dc fault could be detected by using the improved ST analysis combining high frequency information extraction and low frequency information shifting. The following comments are cited on the proposed method, and the results.

1. Compared with the existing ST-based methods, this proposed method could detect various fault transients with a very fast detection speed and sufficient sensitivity. In addition, its validity is less affected by noise. The lightning disturbance could also be identified by using this method. Moreover, its calculation burden on DSP is acceptable, which makes it suitable for dc detection.
2. The selection of identification frequency for low frequency screening is relatively flexible as long as the frequency response of ripple components under normal conditions is considered. However, it should not be a too large value since the spectral leakage caused by fault conditions becomes less obvious in the high frequency band of conventional ST analysis.
3. The steady-state threshold in different systems tends to vary due to different background noise levels. Therefore, in actual use, the steady-state threshold for high frequency detection and low frequency screening should be selected suitably by commissioning based on the local measurement information.
4. According to the instantaneous frequency range of fault current, the optimized sampling frequency could be determined. The correction factor could be chosen as a value close to that range. However, this selection is not strict due to the poor frequency resolution in the high frequency band. By choosing the Nyquist frequency as a value greater than the correction factor, the required sampling frequency could be determined. Overall, increasing sampling frequency could improve the gettable highest time resolution although there would be additional costs. Hence the sampling frequency should be selected appropriately according to the actual demand.
5. A comprehensive comparison between WT, STFT and ST is presented in Figure 25. Overall, this ST method shows a better performance without obvious weaknesses.

VII. CONCLUSION

In this paper, a ST-based dc fault detection method has been proposed with high recognition speed and accuracy. The main contributions are to extract the high frequency information from ST spectrum by introducing a correction factor to detect the accurate fault time due to its high time resolution, and to utilize the low frequency spectrum information to differentiate the fault occurrence, the load change condition and transients on fault-free lines. The effectiveness of this method has been tested in simulation and experiment with the various fault conditions and disturbances. In general, the proposed method is able to provide significantly fast detection speed within 0.3 ms, with clear discrimination between fault transients and normal conditions, high robustness against change of fault conditions, high reliability and acceptable computation burden.

REFERENCES

[1] M. Mazuela, I. Baraia, A. Sanchez-Ruiz, I. Echeverria, I. Torre and I. Atutxa, "Simple Voltage Balancing Method to Protect Series-Connected Devices Experimentally Verified in a 5L-MPC Converter," *IEEE Tr. Ind. Elect.*, vol. 65, no. 5, pp. 3699-3707, 2018.

[2] A. Egea-Alvarez, F. Bianchi, A. Junyent-Ferre, G. Gross, O. Gomis-Bellmunt, "Voltage control of multiterminal VSC-HVDC transmission systems for offshore wind power plants: Design and implementation in a scaled platform," *IEEE Tr. Ind. Elect.*, vol. 60, no. 6, pp. 2381–91, 2013.

[3] C. Guo and C. Zhao, "A new technology for HVDC start-up and operation using VSC-HVDC system," *IEEE Power Energy Soc. Gen. Meet.*, Calgary, 2009.

[4] Y. Xue, Z. Xu, "On the Bipolar MMC-HVDC Topology Suitable for Bulk Power Overhead Line Transmission: Configuration, Control, and DC Fault Analysis," *IEEE Tr. Power Del.*, vol. 29, pp. 2420–29, 2014.

[5] N. Geddada, Y. M. Yeap and A. Ukil, "Fault and load change differentiation in High Voltage Direct Current (HVDC) system," *2016 IEEE Int. Conf. Power Elect. Dr. Energy Sys. (PEDES)*, Trivandrum, 2016.

[6] S. Kantra, H. A. Abdelsalam and E. B. Makram, "Application of PMU to detect high impedance fault using statistical analysis," *IEEE Power Energy Soc. Gen. Meet.*, Boston, 2016.

[7] N. Geddada, Y. M. Yeap, A. Ukil, "Experimental Validation of Fault Identification in VSC-Based DC Grid System," *IEEE Tr. Ind. Elect.*, vol. 65, no. 6, pp. 4799–4809, 2018.

[8] Y. M. Yeap, N. Geddada, A. Ukil, "Analysis and validation of wavelet transform based DC fault detection in HVDC system," *Applied Soft Computing*, vol. 61, pp. 17–29, 2017.

[9] D.K.J.S. Jayamaha, N.W.A. Lidula and A.D. Rajapakse, "Protection and grounding methods in DC microgrids: Comprehensive review and analysis," *Renew. Sustain. Energy Reviews*, vol.120, p. 109631, 2020.

[10] Y. M. Yeap, A. Ukil, "Fault detection in HVDC system using short time Fourier transform," *IEEE Power Energy Soc. Gen. Meet.*, Boston, 2016.

[11] K. Satpathi, Y. M. Yeap, A. Ukil, N. Geddada, "Short-time Fourier transform based transient analysis of VSC interfaced point-to-point dc system," *IEEE Tr. Ind. Elect.*, vol. 65, no. 5, pp. 4080–91, 2018.

[12] R. G. Stockwell, L. Mansinha, R. P. Lowe, "Localization of the complex spectrum: The S transform," *IEEE Tr. Signal Proc.*, vol. 44, pp. 998–1001, 1996.

[13] P. C. Robert, L. Mansinha, "Time-local spectral analysis for non-stationary time series: The S-transform for noisy signals," *Fluctuation and Noise Let.*, vol. 3, pp. 357–64, 2003.

[14] K. Singh and A. Ukil, "Fault Detection in HVDC Transmission Line by S-Transform Technique," *2019 IEEE PES Asia-Pacific Power and Energy Engineering Conference (APPEEC)*, Macao, 2019.
[15] Z. Li, G. Zou, T. Du and W. Yang, "S-transform based pilot protection method for HVDC transmission lines," *2015 5th Int. Conf. Elect. Util. Dere. Restr. Power Tech (DRPT)*, Changsha, 2015, pp. 1667-1672.
[16] Y. Li, S. Lin, R. Tian, X. Lei and Y. Chen, "Pilot Protection Method Based on S Transform Energy Relative Entropy for UHVDC Line," *2nd IEEE Conf. Energy Int. Energy Sys. Int. (EI2)*, Beijing, 2018.
[17] Y. M. Yeap, N. Geddada, K. Satpathi, A. Ukil, "Time- and Frequency-Domain Fault Detection in a VSC-Interfaced Experimental DC Test System," *IEEE Tr. Ind. Inf.*, vol. 14, no. 10, pp. 4353–64, 2018.
[18] Y. M. Yeap, N. Geddada, A. Ukil, "Capacitive discharge based transient analysis with fault detection methodology in dc system," *Int. J. Elect. Power Energy Syst.*, vol. 97, pp. 127–137, 2018.
[19] D. P. Mishra, S. R. Samantaray and G. Joos, "A Combined Wavelet and Data-Mining Based Intelligent Protection Scheme for Microgrid," *IEEE Tr. Smart Grid*, vol. 7, no. 5, pp. 2295-2304, 2016.
[20] W. Li, A. Monti and F. Ponci, "Fault Detection and Classification in Medium Voltage DC Shipboard Power Systems With Wavelets and Artificial Neural Networks," *IEEE Tr. Instr. Meas.*, vol. 63, no. 11, pp. 2651-2665, 2014.
[21] M. Salehi, S. A. Taher, I. Sadeghkhani and M. Shahidehpour, "A Poverty Severity Index-Based Protection Strategy for Ring-Bus Low-Voltage DC Microgrids," *IEEE Tr. Smart Grid*, vol. 10, no. 6, pp. 6860-6869, 2019.
[22] W. R. Gamerota, J. O. Elismé, M. A. Uman and V. A. Rakov, "Current Waveforms for Lightning Simulation," *IEEE Tr. Electromagnetic Compatibility*, vol. 54, no. 4, pp. 880-888, 2012.
[23] W. Xiang, S. Yang, L. Xu, J. Zhang, W. Lin and J. Wen, "A Transient Voltage-Based DC Fault Line Protection Scheme for MMC-Based DC Grid Embedding DC Breakers," *IEEE Tr. Power Del.*, vol. 34, no. 1, pp. 334-345, 2019.
[24] T. Wang, G. Song and K. S. T. Hussain, "Adaptive Single-Pole Auto-Reclosing Scheme for Hybrid MMC-HVDC Systems," *IEEE Tr. Power Del.*, vol. 34, no. 6, pp. 2194-2203, 2019.

Dongyu Li (S'19) received the B.E. degree in Energy and Power Engineering from Northwestern Polytechnical University (NWPU), Xi'an, China, in 2014, and the M.Sc. degree in Sustainable Energy Technology from Xi'an Jiaotong-Liverpool University, Suzhou, China, in 2017.

From 2014–2015, he was working at Daya Bay Nuclear Power Operations and Management Co., Ltd., Shenzhen, China specialising in vibration fault detection. He is currently a doctoral student at the Department of Electrical, Computer and Software Engineering at The University of Auckland (UoA), Auckland, New Zealand. His research interest includes fault detection, localization and isolation in VSC-HVDC system.

Abhisek Ukil (S'05-M'06-SM'10) received the B.E. (1st Class Honors) degree in electrical engineering from the Jadavpur Univ., Kolkata, India, in 2000 and the M.Sc. degree in electronic systems and engineering management from the Univ. of Bolton, Bolton, UK in 2004. He received the Ph.D. degree from the Pretoria (Tshwane) University of Technology, Pretoria, South Africa in 2006, working on automated disturbance analysis in power systems.

Currently, he is Associate Professor in the Dept. of Electrical, Computer and Software Engineering, at The University of Auckland (UoA), Auckland, New Zealand. From 2013–2017, he was Assistant Professor in the School of EEE, Nanyang Technological University, Singapore, where he led a group of 20 researchers with several industrial collaborations. From 2006–2013, he was Principal Scientist at the ABB Corporate Research Center, Baden-Daettwil, Switzerland, where he led several projects on smart grid, protection, control, condition monitoring. He is inventor of 11 patents, and author of more than 180 refereed papers, 2 monographs, 2 chapters. He is associate editor of *IEEE Transactions on Industrial Informatics* & *Springer-Electrical Engineering*. His research interests include smart grid, DC grid, protection & control, renewable energy & integration, energy storage, condition monitoring.

Kuntal Satpathi (S'14-M'18) received the B.Tech. degree in electrical engineering from Haldia Institute of Technology, Haldia, India, in 2011. He received the Ph.D. degree from Nanyang Technological University, Singapore in 2019, working on the operation and fault management of DC marine power system.

From 2011–2014, he was with Jindal Power Limited, Raigarh, India, specializing in thermal power plant operations. Currently, he is a Research Fellow at Nanyang Technological University, Singapore. He is author of more than 18 refereed papers, 1 monograph. His research interests include modeling, control, and protection of AC/DC grids.

Yew Ming Yeap (S'14-M'18) received the B.Eng (1st Class Honors) degree in Electrical Engineering from the University of Malaya, Kuala Lumpur, Malaysia, in 2013. He received the Ph.D. degree from the Nanyang Technological University, Singapore, in 2018, working on fault detection in High Voltage Direct Current (HVDC) systems.

Currently, he is a Scientist at the Institute for Infocomm Research (I2R), Singapore, and leading an industry project on EV as co-Principal Investigator. He is author of more than 20 refereed papers, 1 monograph. His research interests include DC grid, smart grid, power electronics & control, energy storage for EV.